Numerical Simulation of Viscoelastic Fluid Flow Past a Cylinder

R. Kharrat[1] and S. Vossoughi[2]

Numerical methods have been applied to the flow problems of viscoelastic fluids for some considerable time. However, many of the theoretical predictions do not agree with experimental observation. This is even true for the simple geometry such as viscoelastic liquids past a single cylinder. Among the different numerical schemes considered, the method of lines was found to be the most promising. In this method, the partial differential equations were reduced to a system of ordinary differential equations and then the resulting system of equations was solved using the Runge-Kutta method. Consistent with the available literature data, a downstream shifting of the streamlines was found for low elasticity while for the high elasticity the streamline shifting was pronounced at upstream. The pressure and vorticity distribution around the surface of the cylinder was found to alter in the presence of shear-thinning parameter. Solution was found to be mesh size dependent; hence, caution should be exercised to avoid the numerical artifact.

INTRODUCTION

In the last decade, a considerable effort has been dedicated to the prediction of viscoelastic behavior exhibited by polymer solutions and melts and its impact on polymer processing. This behavior becomes most evident in non-viscometric flows such as the entry flow through an abrupt contraction and the die exit flow encountered in all extrusion operations.

The flow of viscoelastic fluids over a cylinder is an idealization of the flow situation commonly encountered in industrial processing. It is, furthermore, a flow configuration which has been studied with a great detail for Newtonian fluids–both experimentally and theoretically–and which can be used as a base of comparison with the viscoelastic fluid flow.

Due to the complexity of the equations involved, most efforts have been directed toward numerical techniques and several investigations have been reported in the literature [1–4]. From the review of the literature, the following facts emerged:

1. Numerical schemes "diverge" for comparatively low elasticity values. In addition, it has been found very difficult to obtain solutions for flows of highly viscoelastic liquids; consequently, smoothing procedures and transient solutions have been recommended.
2. The numerical schemes predict a downstream shift of the streamlines for the low values of the viscoelastic parameters, such as relaxation time and retardation time.

1. University of the Petroleum Industry, Abdullah Coute, Ahwaz, I.R. Iran.
2. Department of Chemical and Petroleum Engineering, University of Kansas, Lawrence, KS 66045, USA.

Scientia Iranica, Vol. 1, No. 3, © Sharif University of Technology, October 1994.

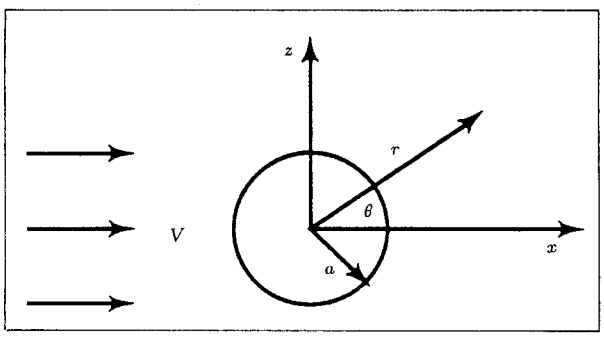

Figure 1. Coordinate system.

However, no numerical technique has yet been devised to predict the upstream shifting associated with the high values of the viscoelastic parameters.

The transient solution of the viscoelastic fluid past a cylinder has its own stability and divergence problems as well as truncation errors. The objective of this work is to try different schemes of finite difference methods, in search of the most effective one in solving the partial differential equations describing the flow of viscoelastic liquid past a cylinder.

BASIC EQUATIONS AND THEORY

The unsteady state flow of an incompressible viscoelastic liquid past a cylinder of radius "a" and of infinite length is considered. All motions are referred to as a set of cylindrical polar coordinates (r, θ, z), where the z axis coincides with the axis of the cylinder as shown in Figure 1. At a large distance from the cylinder, the flow of liquid is assumed to be constant with an approaching velocity, V, in the positive x-direction. The equations of continuity, momentum, and an implicit four-constant time dependent Oldroyd rheological equation of state are used to describe the flow of viscoelastic fluid flow past a cylinder. In addition, the concepts of vorticity and stream functions are employed. The appropriate boundary conditions on the cylinder and at infinity are used to complete the specification of the problem. The detail analysis and derivation is given in Appendix I. It should be noted that the Oldroyd model is employed to be able to observe the viscoelastic effect in the presence and absence of the shear-thinning effect by varying the corresponding parameters independently.

METHODS OF SOLUTION

In order to discretize the equations, some finite-difference grids need to be adopted. Since it is desirable to have a finer mesh near the cylinder surface, an exponential transformation of the r-coordinate, as given in Appendix II, was considered. Because of the symmetry, only half of the cylinder needs to be considered. The finite-difference grid for half of the cylinder is given in Figure 2.

Initially, the equation of state was solved by direct iteration and the stream function by the point relaxation method. This approach has been adopted by several investigators for steady state flow of viscous and viscoelastic fluid around an object. Two problems were encountered during the computation process, one being large computation time and the second, lack of convergence at moderate values of Reynolds numbers.

The second approach was to solve the problem using the alternating direction method for the equation of state. This method makes use of splitting the time step to obtain a multi-dimensional implicit method which requires only the inversion of a tri-diagonal matrix. This approach is currently the most popular method to viscous problems. Although the computation time was reduced, the divergence

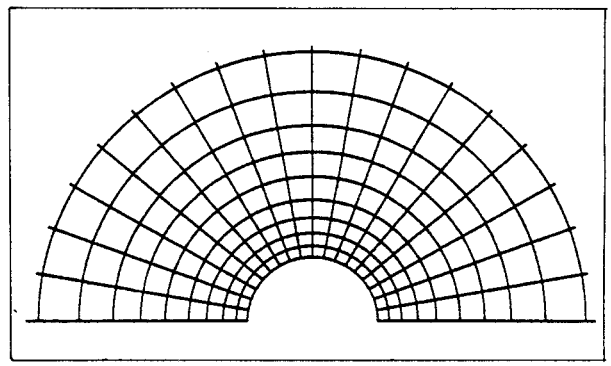

Figure 2. Finite-difference grid.

Table 1. Programs description.

Program Name	Subroutine	Method of Solution
PROG.OLD	Stream Rheology Vorticity	Point Relaxation Direct Iteration Alternating Direction
PROG.ADI	Stream Rheology Vorticity	Point Relaxation Alternating Direction Alternating Direction
PROG.GIL	Stream Rheology Vorticity	Point Relaxation Runge-Kutta-Gill Runge-Kutta-Gill
PROG.FUL	Stream Rheology Vorticity	Point Relaxation Fully Implicit Fully Implicit

problem at moderate values of Reynolds numbers persisted. To remedy the problem, the mesh size and time steps had to be reduced, which in turn increased the computation time substantially.

In the third approach, a fully implicit method was tried. Although this method was more stable and the solution converged at moderate values of Reynolds numbers, its long computation time restricted its usage.

The final approach was to improve the accuracy of the time derivative terms by introducing higher order of truncation. The method of lines was then adopted. The computation time was significantly reduced in comparison to the other techniques and no divergence problem was observed for moderate values of Reynolds numbers and elasticity parameters. Still finer mesh sizes and smaller time steps had to be used for high values of Reynolds numbers and elasticity parameters.

Table 1 identifies the names, subroutines and methods used in each program generated in this work. The numerical methods used in each program will be briefly discussed in the following paragraphs. Complete discussion of the numerical techniques employed in this work is given elsewhere [4].

PROG. OLD

In this program, the stream function is solved using the point relaxation method. The basic theme of this method is to begin the solution with initial estimate values for the dependent variable and to use repeated substitution and recalculation to arrive at the converged values. The criterion for convergence involved a requirement that two successive iterates differ by less than an assigned tolerance.

A direct iterative method was used to solve the stress equations. The derivatives are represented by either forward or backward differences or a combination of the two, so that the resulting algebraic equations are diagonally dominant. A single iteration loop incorporates all three equations and they are solved simultaneously. The vorticity equation is solved using the Alternating Direction/Implicit (ADI) method.

PROG. ADI

In this program, the stream equation is solved as before, whereas the vorticity and the three stress equations are solved using the ADI method.

PROG. GIL

In this program, the point relaxation method is used for the stream function, whereas the Runge-Kutta-Gill method is used for the vorticity and the three stress equations. The partial differential equations are reduced to ordinary differential equations. The central difference is the space derivative used, which gives a second-order truncation error while the time derivative is fourth-order using the Runge-Kutta method.

PROG. FUL

In this program, the fully implicit method is used for the three subroutines. Here, all variables are evaluated at the same time step, while in the other programs the stream function always lags in time. In the formulation of the

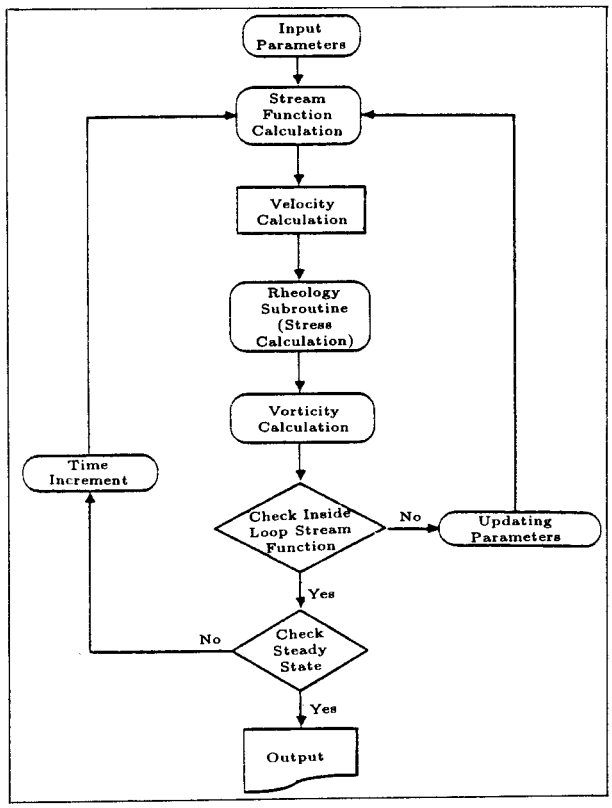

Figure 3. Flow chart of the simulator.

fully implicit method, a general penta-diagonal matrix is generated. The solution of the matrix is obtained by using a Bandmatrix program. Another approach to the problem is to reduce the penta-diagonal to a tri-diagonal matrix and to solve it with the Thomas algorithm. In this case, the values of the unknown parameters at the deleted diagonals are taken at previous iteration.

Various steps involved in the numerical solution process can be conveniently discussed by reference to the flow chart given in Figure 3. The algorithm is started with the initial values and the known boundary conditions. The subsequent sequence of events is summarized below:

1. Calculate the stream function.
2. Compute the vorticity on the surface using the calculated stream function values from step 1.
3. Calculate the velocities u and v from the known values of the stream function.
4. Calculate the three stresses on the boundary.
5. Calculate the three stresses in the domain using the calculated stresses from step 4 and the known velocities and stream functions.
6. Compute the vorticity in the domain using the known values of the stresses and velocities.
7. Check on the convergence of the vorticity values on the surface if required (this is the inside loop).
8. Check the steady state condition if required.
9. Increment the time.
10. Repeat all steps until the selected time is approached.
11. Print results.

GENERAL STRATEGY

As mentioned in Appendix II, one of the boundary conditions for vorticity requires its value being zero for all the time at $r = R_\infty$. However, since the vortex moves with time toward the boundary, the outer boundary distance, R_∞, used for the calculations must be chosen large enough so that the condition of vorticity at the boundary is not violated. The steady state condition was established by checking the value of the total drag in several consecutive time steps being approximately the same.

The various computer programs were checked against Newtonian fluid flow by setting the elastic parameters in the rheological equation of state equal to zero. This is because of the stress contribution from elasticity being zero for the case of Newtonian fluid.

To achieve stability, the mesh sizes, especially in the normal direction, had to be reduced with increasing Reynolds number and the time steps had to be reduced at low Reynolds numbers. For every Reynolds number, the stability

and convergence of the solution is established first through the appropriate selection of mesh sizes and time steps, then the elastic parameters were considered. For a given computation time the solution for the Newtonian case was found to converge faster than the solution for the viscoelastic case.

INVISCID FLOW RESULTS

The analytical solution of the potential flow of an inviscid fluid past a cylinder is well known. Streamlines were generated numerically and compared with the analytical solution. The agreement was satisfactory and the relative error was found to be less than 1% for all the stream functions investigated.

VISCOUS FLOW RESULTS

Figures 4 and 5 compare the vorticity and pressure distribution on the surface of the cylinder respectively with those of Apelt [5] for the steady state case. It is evident that the present work is in good agreement with the work of previous investigators. It should be noted that the steady state solution in the present work was obtained from the transient solution. Also a drag coefficient of 1.51 and an angle of separation of 50° were obtained which were in good agreement with the reported values in the literature.

The transient solution was compared with the work of Son and Hanratty [6] for Reynolds number of 20. Comparisons were made for the pressure and the vorticity distribution on the cylinder surface and for the streamlines projection. Figures 6 and 7 compare the pressure distribution on the cylinder surface. For the sake of keeping the length of the paper reasonable, the other figures are not included. Good agreement was achieved in all cases. Consistent with their work, the point of separation of the zero streamline from the surface of the cylinder was observed. In addition, the formation of the dead zone was also noticeable.

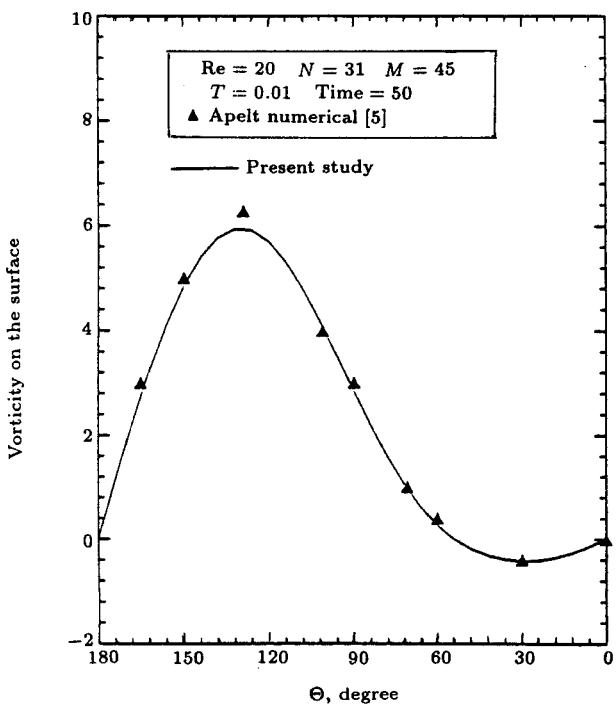

Figure 4. Vorticity distribution on the cylinder surface.

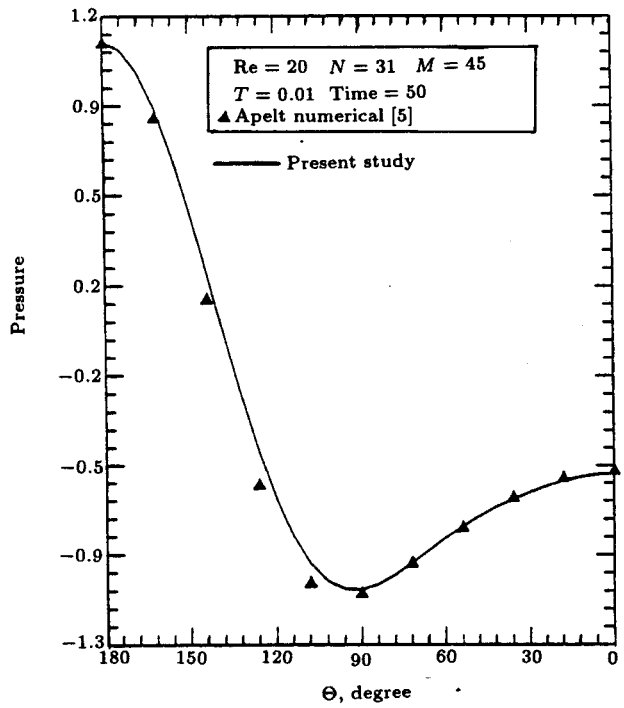

Figure 5. Pressure distribution on the cylinder surface.

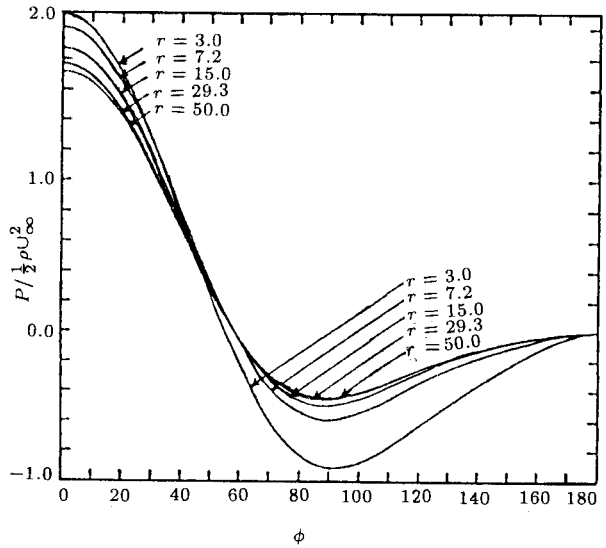

Figure 6. Numerical solution for flow around a cylinder [6].

VISCOELASTIC FLUID FLOW RESULTS

In comparing the performance of the different numerical schemes, a base case of the Reynolds number of 2.5, the elastic parameters of 0.6 and 0.1 for the relaxation time and the retardation time respectively, were considered. These values were used in the work of Townsend [3] for the viscoelastic fluid flow over a fixed and rotating cylinder. The adaption of these values will provide a useful comparison with the results of this work.

Figure 8 shows the variation of the total drag on the cylinder surface with time calculated by different methods. As noticed, all the methods employed produced practically the same solution. However, the CPU time of 5.84 minutes for the method of lines was lowest among the other two, namely, alternating direction being 6.19 minutes and the fully implicit 32.33 minutes. All the computations were carried out on the Harris 1200 and 800 at the University of Kansas.

In order to reduce the computation time of the fully implicit program, the penta-diagonal matrix was reduced to a tri-diagonal matrix as mentioned earlier. This approach reduced the computation time by a factor of 13. In addition to this change, the inside loop as portrayed by Figure 3 was omitted by taking small time steps to accommodate the fast changes in the flow. Due to this modification, the computation time was further reduced by a factor of three. The total drag variation on the cylinder surface with time up to a dimensionless time of 1.0

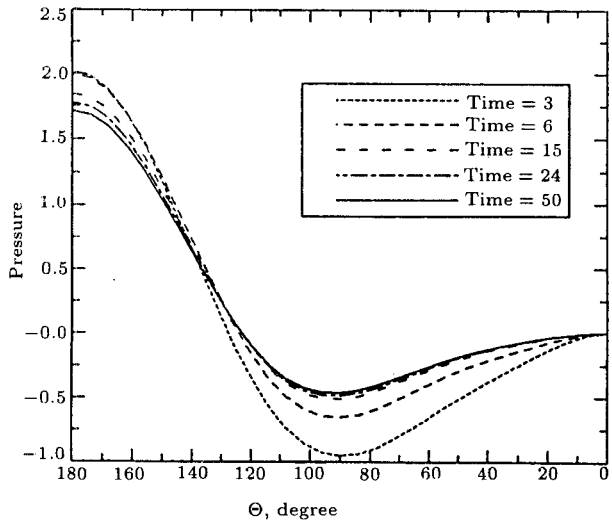

Figure 7. Pressure distribution on the cylinder surface for Re = 20, present study.

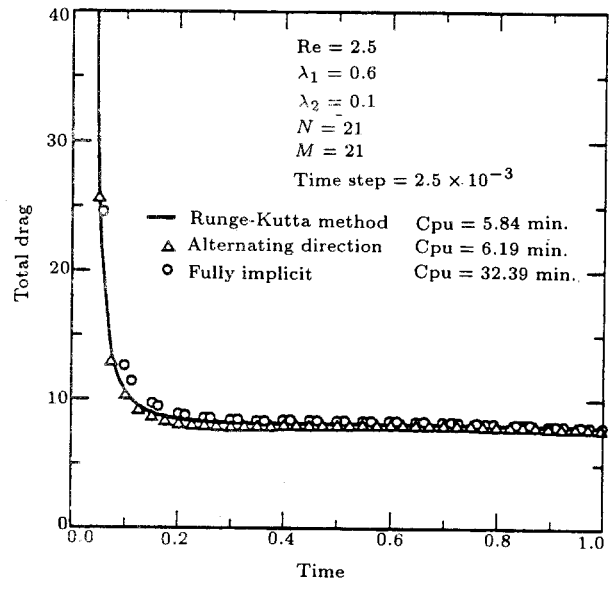

Figure 8. Comparison of the different methods of solution.

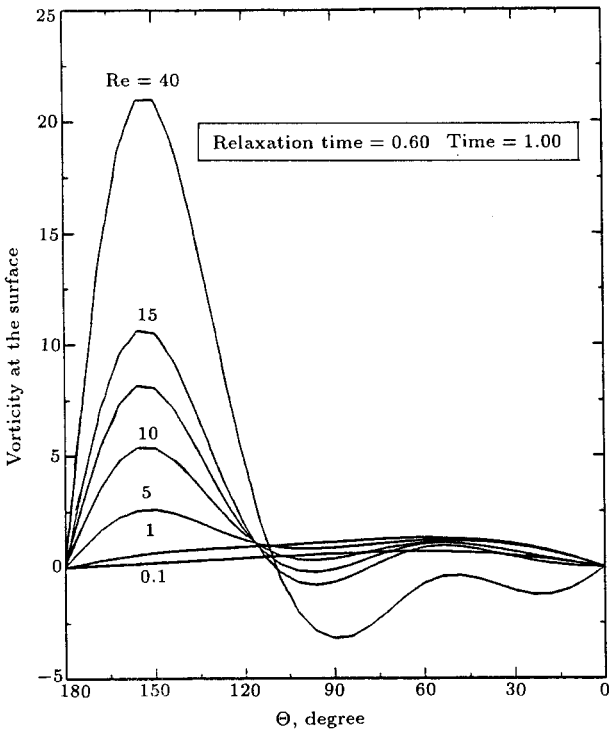

Figure 9. Vorticity distribution on the cylinder surface.

was generated using the three modified fully implicit schemes. The close agreement provided confidence in a semi-fully implicit method that gave acceptable results.

The effect of the Reynolds number on the flow of an elastic fluid with a relaxation time of 0.6 was studied in terms of the vorticity, pressure and the total drag distribution on the cylinder surface. Figure 9 presents the vorticity distribution. Higher vorticity values result from higher Reynolds numbers. The negative and positive values refer to clockwise and counterclockwise motions respectively.

In the case of the pressure distribution (figure not given), as the Reynolds number increased, the pressure decreased. Major changes occurred for the Reynolds number in the range of 0.1 to 1.0. The location of the maximum pressure remained insensitive to the magnitude of the Reynolds number.

The total drag (figure not given) increased with increasing Reynolds number. This was much more pronounced for Reynolds numbers smaller than 1.0. Total drag became relatively

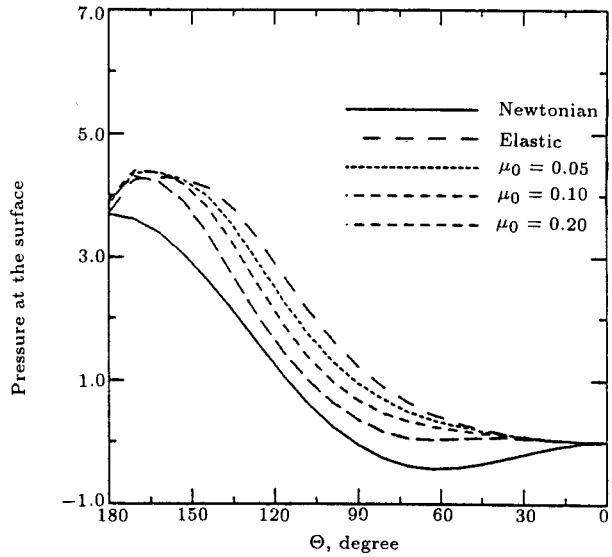

Figure 10. Effect of shear-thinning on the pressure distribution for Re = 2.5, $\lambda_1 = 2$ and $\lambda_2 = 1$.

insensitive to Reynolds numbers in the range of 5 through 40.

The effects of the shear-thinning parameter, μ_0, on the pressure and vorticity distribution are shown in Figures 10 and 11, respectively. These figures were generated for $\lambda_1 = 2$, $\lambda_2 = 1.0$ and Reynolds number of 2.5. As observed in Figure 10, higher value of shear-

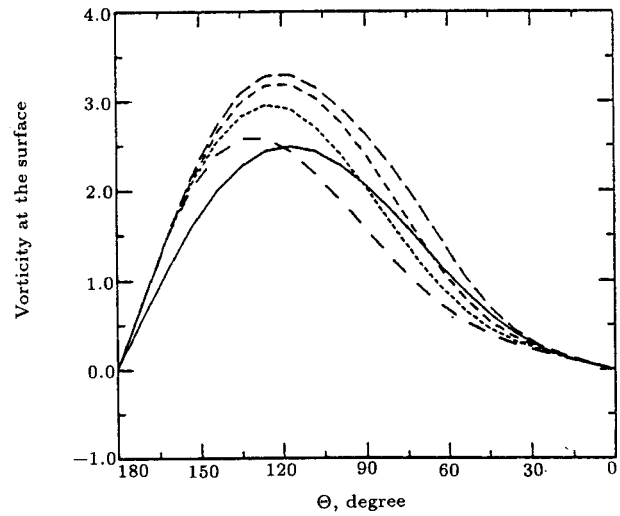

Figure 11. Effect of shear-thinning on the vorticity distribution for Re = 2.5, $\lambda_1 = 2$ and $\lambda_2 = 1$.

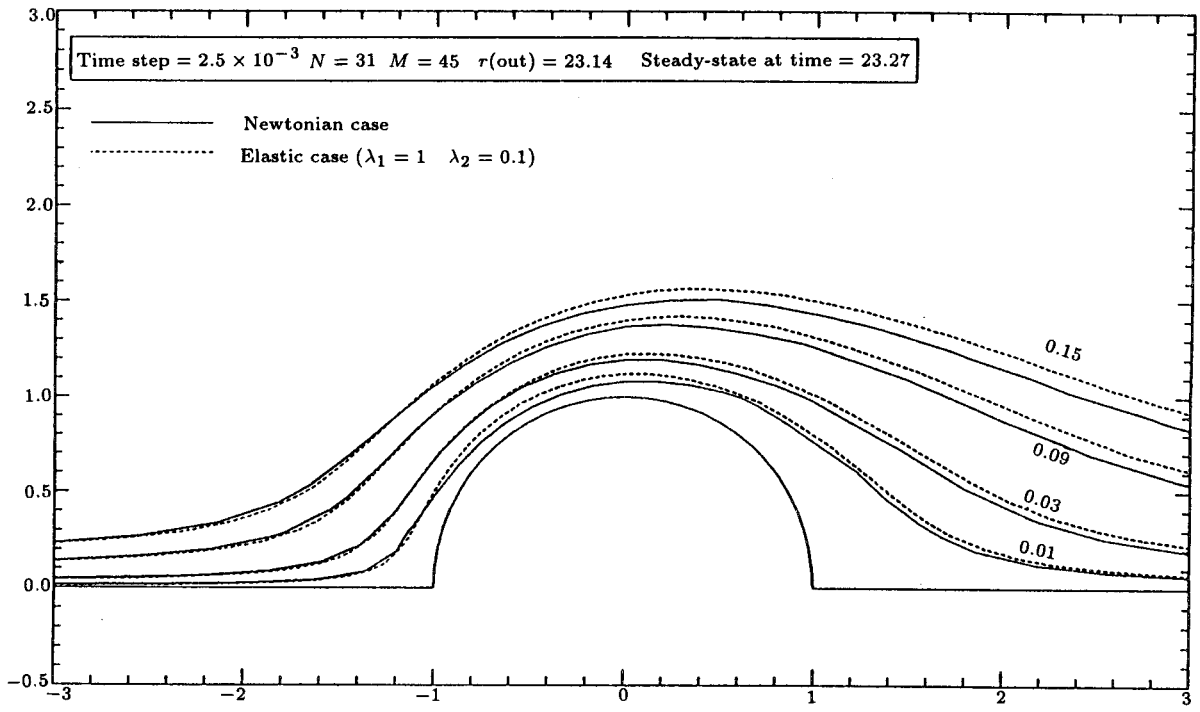

Figure 12. Comparison of elastic and Newtonian streamline patterns for Reynolds number 2.5 ($\lambda_1 = 1$, $\lambda_2 = 0.1$).

thinning parameter lowered the maximum pressure. However, the maximum vorticity value increased as the shear thinning parameter was increased. Hence, the shear-thinning parameter might enhance the rotation of the fluid particles which is manifested in the vorticity value.

The effect of the retardation time, λ_2, on the pressure and vorticity distribution was also studied. The figures generated (not given here) indicated that, as the value of λ_2 increased, the maximum pressure decreased. In the case of the vorticity distribution, the maximum value shifted toward the upstream region, approaching that of the Newtonian case as the value of λ_2 increased.

The downstream and upstream shifting of the streamlines was studied by considering small and large relaxation times. Streamline profiles for Newtonian and viscoelastic fluid with small relaxation time were generated. The pattern of the streamlines indicated a downstream shift relative to Newtonian, as reflected in Figure 12. This result compares favorably with those of Pilate and Crochet [7] and with those of Townsend [8]. The upstream shifting is noticed in Figure 13, which was generated for the highly viscoelastic fluid. This is in agreement with the experimental observations of Manero and Mena [9]. The viscoelastic parameters used in this work are equivalent and comparable to the Weissenberg number used by Manero and Mena.

Solutions were also generated for the Newtonian, elastic and viscoelastic fluids by setting the appropriate parameters of λ_1, λ_2, and μ_0 to zero. The total drag on the cylinder versus time is given in Figure 14. In all cases, the drag value starts at a maximum value at the initiation of flow and levels off to a steady state value. The higher drag for the elastic fluid is consistent with what is reported in the literature. Figure 15 is a similar plot generated for much smaller Reynolds number and larger relaxation time. A slight decrease in the total drag is noticed at a dimensionless time of 20, at which, steady state is presumably reached. A decrease in the total drag has been reported in the literature at low Reynolds numbers [3].

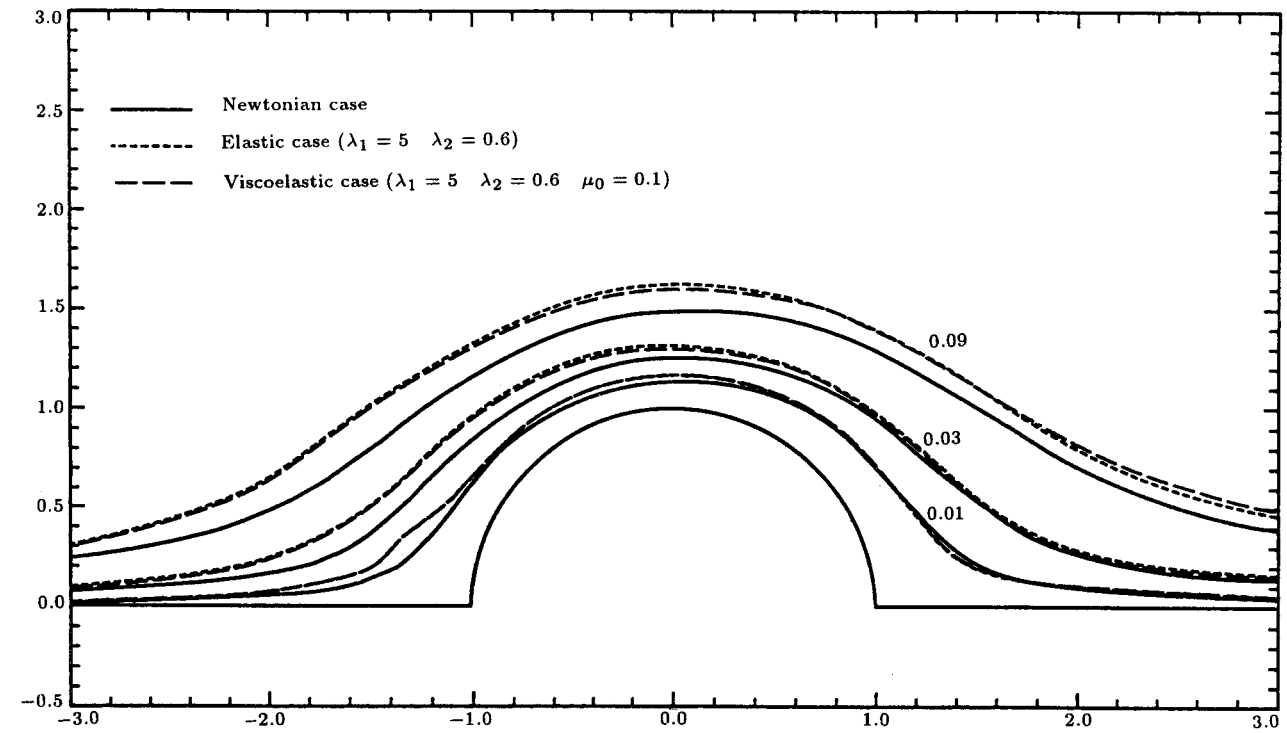

Figure 13. Newtonian, elastic and viscoelastic streamlines projection for Reynolds number 0.25.

Effect of Mesh Size

A highly viscoelastic fluid with a Reynolds number of 2.5 was considered to study the transient behavior of the flow. Figure 16 shows the streamlines in the early stages of the flow at a dimensionless time of 1.2. The development of a dead zone is evident. This zone is marked by the zero streamline in the downstream region and moves in the opposite direction of the flow at the later stages. At a later dimensionless time of 5, the streamline projection revealed the existence of two dead zones in the upstream

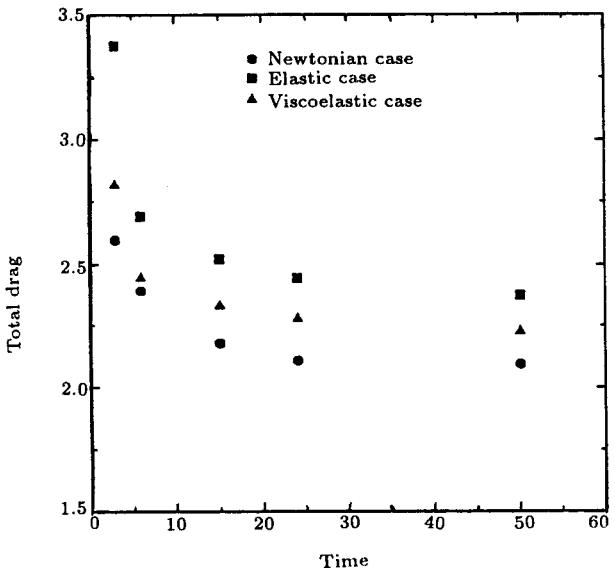

Figure 14. Total drag variation through time for Re = 10 ($\lambda_1 = 0.6, \lambda_2 = 0.1, \mu_o = 0.1$).

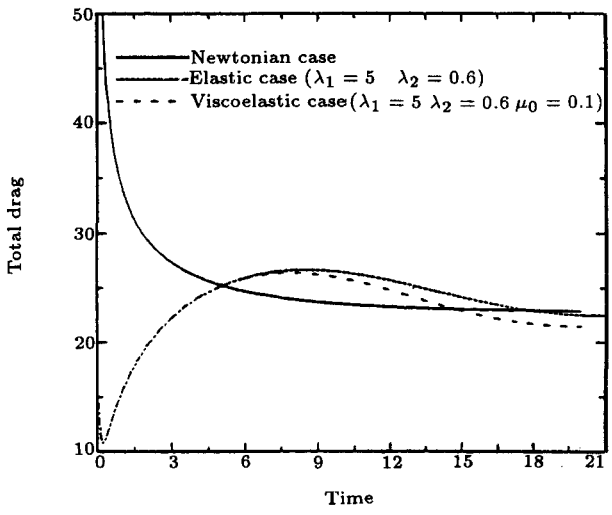

Figure 15. Total drag variation through time for Re = 0.25 ($\lambda_1 = 5, \lambda_2 = 0.6, \mu_o = 0.1$).

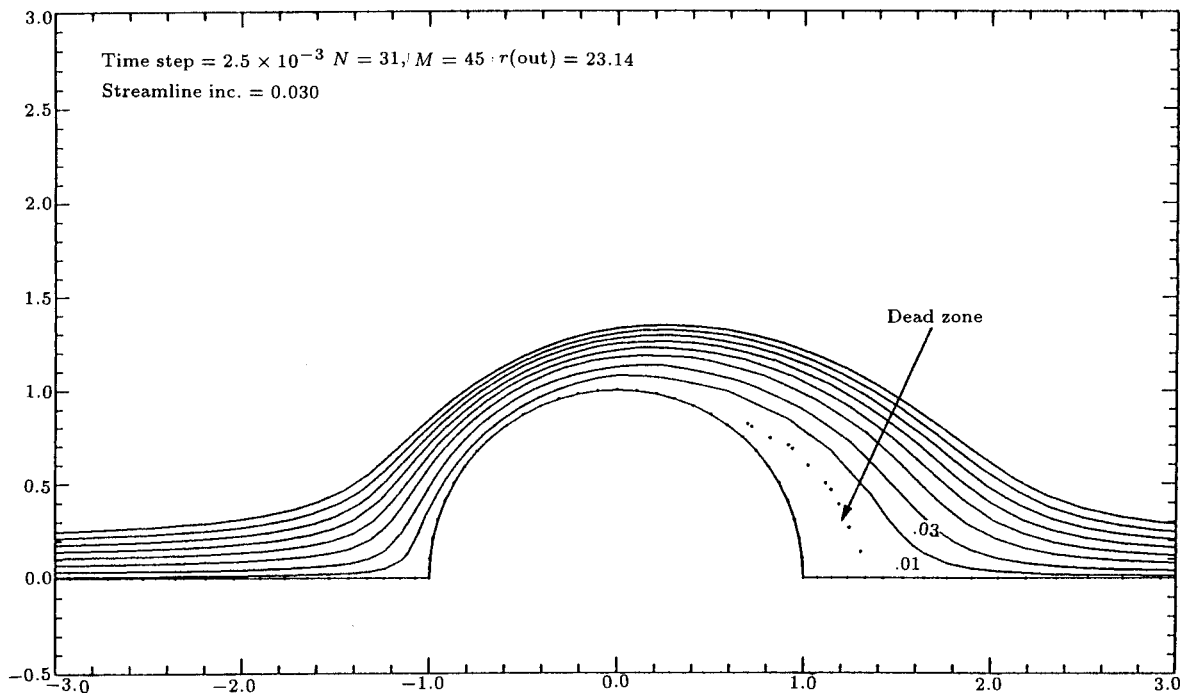

Figure 16. Streamline patterns for Re = 2.5, $\lambda_1 = 5, \lambda_2 = 0.6$ and time = 1.2 .

region. The question was raised as to whether the observed behavior was a numerical artifact. Hence, the mesh size reduction in both the normal and the angular direction was considered. In the case of the latter, no noticeable changes were observed. However, the variation of the mesh size in the normal direction affected the size of the dead zone considerably. Smaller mesh size also extended the transient solution over a longer period of time.

The observation of the dead zone has also been reported in the numerical work of Townsend [8]. He considered the dead zone to be due to the viscoelastic behavior of the fluid.

CONCLUSIONS

The method of lines was found to be the most effective approach for solving the viscoelastic fluid flow equations over a cylinder. The numerical results compare favorably with the experimental evidence. Upstream and downstream shifting of streamlines was detected. It was also noticed that the presence of the shear thinning component altered the pressure and vorticity profiles to some extent. Small decrease in drag in presence of elasticity was predicted for Re << 1 while an increase in drag in presence of elasticity was predicted for Re >> 1. Finally, the results of the numerical solution were found to be mesh-size dependent.

REFERENCES

1. Leslie, F.M. "The flow of a viscoelastic fluid past a sphere", *J. Mech. Math.*, **14**, p 36 (1961).

2. Ultman, J.S. and Denn, M.M. "Slow viscoelastic flow past submerged objects", *The Chemical Eng. J.*, **2**, p 81 (1971).

3. Townsend, P. "A numerical simulation of Newtonian and viscoelastic flow past stationary and rotary cylinders", *J. non-Newtonian Fluid Mech.*, **6**, p 219 (1980).

4. Kharrat, R. "Rheological characterization of a Boger fluid and the numerical simulation of its flow across a cylinder", Ph.D. dis-

sertation, The University of Kansas, USA (1989).

5. Apelt, H.A. "The steady flow of a viscous fluid past a circular cylinder at Reynolds numbers 40 and 44", A.R.C. Tech. Rep., R. & M., No. 3175 (1961).

6. Son, J.S. and Hanratty, T.J. "Numerical solution for flow around a cylinder at Reynolds numbers of 40, 200 and 500", *J. Fluid Mech.*, **35**, part 2, p 369 (1969).

7. Pilate, G. and Crochet, M.J. "Plane flow of a second-order fluid past submerged boundaries", *J. non-Newtonian Fluid Mech.*, **2**, p 323 (1977).

8. Townsend, P. "On the numerical simulation of two dimensional time dependent flow of Oldroyd fluids, part 1: basic method and preliminary results", *J. non-Newtonian Fluid Mech.*, **14**, p 265 (1984).

9. Manero, O. and Mena, B. "On the flow of viscoelastic fluid in cross flow around a circular cylinder", *J. non-Newtonian Fluid Mech.*, **9**, p 379 (1981).

APPENDIX I

System of Equations

The equations of momentum and continuity are:

$$\rho[\frac{\partial u}{\partial t}+u\frac{\partial u}{\partial r}+\frac{\partial u}{\partial \theta}-\frac{v^2}{r}]= -\frac{\partial p}{\partial r}+\frac{\partial T_{rr}}{\partial r}+\frac{1}{r}\frac{\partial T_{\theta\theta}}{\partial \theta}+\frac{1}{r}(T_{rr}-T_{\theta\theta}), \quad \text{(I.1)}$$

$$\rho[\frac{\partial v}{\partial t}+u\frac{\partial v}{\partial r}+\frac{v}{r}\frac{\partial v}{\partial \theta}+\frac{uv}{r}]= \frac{1}{r}\frac{\partial p}{\partial \theta}\frac{\partial T_{r\theta}}{\partial r}+\frac{2}{r}T_{r\theta}+\frac{1}{r}\frac{\partial T_{\theta\theta}}{\partial \theta}, \quad \text{(I.2)}$$

$$\frac{\partial u}{\partial r}+\frac{u}{r}+\frac{1}{r}\frac{\partial v}{\partial \theta}=0, \quad \text{(I.3)}$$

where ρ is the density of the liquid, u and v are the velocity in the r and θ direction respectively, p denotes the isotropic pressure, and T_{rr}, $T_{\theta\theta}$ and $T_{r\theta}$ are the relevant components of the extra stress tensor. The fluid is characterized by the rheological equation of state:

$$T_{ik}+\lambda_1\frac{\vartheta}{\vartheta t}T_{ik}+\mu_0 T_j^j D_{ik}= 2\eta_0[D_{ik}+\lambda_2\frac{\vartheta}{\vartheta t}D_{ik}], \quad \text{(I.4)}$$

where λ_1, λ_2 and μ_0 are material time constants, D_{ik} is the rate-of strain tensor, and $\vartheta/\vartheta t$ is the co-deformational derivative. When operating on a contravariant tensor, the co-deformational operator produces:

$$\frac{\vartheta}{\vartheta t}T_{ik}=\frac{\partial}{\partial t}T_{ik}+v^n\frac{\partial T_{ik}}{\partial x^m}-\frac{\partial v}{\partial x^m}T_{im}-\frac{\partial v^i}{\partial x^m}T_{mk}. \quad \text{(I.5)}$$

To complete the specification of the problem, we need appropriate boundary conditions on the cylinder and at infinity. Initially, the fluid is assumed to be at rest but subsequently, the boundary conditions are given by:

$$\begin{aligned} &u=v=0, && 0<\theta<\pi, && r=a,\\ &u=v\cos\theta, && 0<\theta<\pi, && r=R_\infty,\\ &v=-v\sin\theta, && 0<\theta<\pi, && r=R_\infty,\\ &v=0, && \theta=0 \text{ and } \pi. && \end{aligned} \quad \text{(I.6)}$$

At the far boundary, $r = R_\infty$, the flow is assumed to be steady, unidirectional and not influenced by elasticity. We may therefore have:

$$T_{rr}=T_{\theta\theta}=T_{r\theta}=0. \quad \text{(I.7)}$$

The boundary condition for the stresses on the cylinder surface and the symmetry lines were obtained using the velocity conditions.

Before attempting to solve the system of Equations I.1–I.4, a number of simplifications were made. First, the stream function, Ψ, defined by Equation I.8, was introduced:

$$u=\frac{1}{r}\frac{\partial \Psi}{\partial \theta}, \quad v=-\frac{\partial \Psi}{\partial r}. \quad \text{(I.8)}$$

Equation I.8 satisfies the equation of continuity. Second, the following non-dimensional variables were introduced:

$$r^* = r/a; \quad u^* = u/V; \quad v^* = v/V;$$
$$T^*_{ik} = T_{ik}a/\eta_0 V; \quad \Psi^* = \Psi/aV; \quad \lambda^*_1 = \lambda_1 V/a;$$
$$\lambda^*_2 = \lambda_2 V/a; \quad t^* = tV/a; \quad p^* = p/\rho V^2. \tag{I.9}$$

For the sake of convenience, the $*$'s are dropped although non-dimensionality is implied. In addition, the following changes of variables were also made:

$$T_{rr} = \overline{T}_{rr} + 2\frac{\partial u}{\partial r},$$
$$T_{\theta\theta} = \overline{T}_{\theta\theta} + 2(\frac{1}{r}\frac{\partial v}{\partial \theta} + \frac{u}{r}),$$
$$T_{r\theta} = \overline{T}_{r\theta} + r\frac{\partial}{\partial r}(\frac{v}{r}) + \frac{1}{r}\frac{\partial u}{\partial \theta}. \tag{I.10}$$

The tensor $\overline{T}_{ik}$ represents a deviation from Newtonian flow behavior. The above transformation introduces a vorticity diffusion term in the vorticity equation which will be given later.

The pressure is eliminated from Equation I.1 and I.2 by cross-differentiating Equation I.1 with respect to θ and Equation I.2 with respect to r to yield the vorticity and stream function equations. It should be noted that the bar notation is dropped for the sake of convenience and the definition is still applied:

$$\frac{\partial \omega}{\partial r} + \frac{1}{r}[\frac{\partial \Psi}{\partial \theta}\frac{\partial \omega}{\partial r} - \frac{\partial \Psi}{\partial r}\frac{\partial \omega}{\partial \theta}] - \frac{1}{Re}\nabla^2\omega =$$
$$\frac{1}{Re}\{\frac{1}{r}\frac{\partial}{\partial \theta}[\frac{\partial T_{rr}}{\partial r} + \frac{1}{r}\frac{\partial T_{r\theta}}{\partial \theta} + \frac{T_{rr} - T_{\theta\theta}}{r}]$$
$$- \frac{1}{r}\frac{\partial}{\partial r}[r(\frac{\partial T_{r\theta}}{\partial r} + 2\frac{T_{r\theta}}{r} + \frac{1}{r}\frac{\partial T_{\theta\theta}}{\partial \theta})]\}, \tag{I.11}$$

where $Re(= \rho aV/\eta_0)$ is the Reynolds number, ∇^2 is the usual Laplacian operator and ω is the magnitude of the vorticity vector and is given by:

$$\omega = \nabla^2\Psi. \tag{I.12}$$

Equation I.4, after being written in non-dimensional form and implementing the change of variables, produces the following three components:

rr-component:

$$[1 - \frac{\partial u}{\partial r}(2\lambda_1 - \mu_0)]T_{rr} + \lambda_1[\frac{\partial T_{rr}}{\partial t} + u\frac{\partial T_{rr}}{\partial r}$$
$$+ \frac{v}{r}\frac{\partial T_{rr}}{\partial \theta}] - \frac{2\lambda_1}{r}\frac{\partial u}{\partial \theta}T_{r\theta} + \mu_0\frac{\partial u}{\partial r}T_{\theta\theta} =$$
$$2(\lambda_2 - \lambda_1)\{\frac{\partial^2 u}{\partial r \partial t} + u\frac{\partial^2 u}{\partial r^2}$$
$$+ \frac{v}{r}\frac{\partial^2 u}{\partial r \partial \theta} - 2(\frac{\partial u}{\partial r})^2 - \frac{\partial u}{\partial \theta}$$
$$(\frac{\partial u}{\partial \theta}[\frac{\partial u}{\partial r}(\frac{v}{r}) + \frac{1}{r^2}\frac{\partial u}{\partial \theta}])\}, \tag{I.13}$$

$\theta\theta$-component:

$$[1 + \frac{\partial u}{\partial r}(2\lambda_1 - \mu_0)]T_{\theta\theta} + \lambda_1[\frac{\partial T_{\theta\theta}}{\partial t} + u\frac{\partial T_{\theta\theta}}{\partial r}$$
$$+ \frac{v}{r}\frac{\partial T_{\theta\theta}}{\partial \theta}] - 2\lambda_1(\frac{\partial v}{\partial r} - \frac{v}{r})T_{\theta\theta} - \mu_0 T_{rr}\frac{\partial u}{\partial r} =$$
$$2(\lambda_2 - \lambda_1)r^2[\frac{\partial}{\partial t}(\frac{1}{r^3}(u + \frac{\partial v}{\partial \theta}))$$
$$- 2\frac{\partial}{\partial \theta}(\frac{v}{r})(\frac{1}{r^3}(u + \frac{\partial v}{\partial \theta}))], \tag{I.14}$$

$r\theta$-component:

$$T_{r\theta} + \lambda_1[\frac{\partial T_{r\theta}}{\partial t} + u\frac{\partial T_{r\theta}}{\partial r} + \frac{v}{r}\frac{\partial T_{\theta\theta}}{\partial \theta}] - \frac{\lambda_1}{r}\frac{\partial u}{\partial \theta}T_{\theta\theta}$$
$$- \lambda_1 T_{rr}(\frac{\partial v}{\partial r} - \frac{v}{r}) + \frac{\mu_0}{2}(T_{rr} + T_{\theta\theta})$$
$$(\frac{\partial v}{\partial r} - \frac{v}{r} + \frac{1}{r}\frac{\partial u}{\partial \theta}) = (\lambda_2 - \lambda_1)r$$
$$[(\frac{\partial}{\partial t}(\frac{\partial}{\partial r}(\frac{v}{r}) + \frac{1}{r^2}\frac{\partial u}{\partial \theta}) + \frac{v}{r}\frac{\partial}{\partial \theta}$$
$$(\frac{\partial}{\partial r}(\frac{v}{r}) + \frac{1}{r^2}\frac{\partial u}{\partial \theta}) - \frac{\partial u}{\partial r}(\frac{\partial}{\partial r}(\frac{v}{r})$$
$$+ \frac{1}{r^2}\frac{\partial u}{\partial \theta}) - 2\frac{\partial u}{\partial \theta}(\frac{1}{r^3}(u + \frac{\partial v}{\partial \theta})) - 2\frac{\partial}{\partial r}$$
$$(\frac{v}{r})\frac{\partial u}{\partial r} - \frac{\partial}{\partial \theta}(\frac{v}{r})(\frac{\partial}{\partial r}(\frac{v}{r}) + \frac{1}{r^2}\frac{\partial u}{\partial \theta})]$$
$$+ u\frac{\partial}{\partial r}(\frac{\partial}{\partial r}(\frac{v}{r}) + \frac{1}{r^2}\frac{\partial u}{\partial \theta})]. \tag{I.15}$$

For the Newtonian case, λ_1, λ_2 and μ_0 are zero and Equations I.13-I.15 are trivially satisfied.

APPENDIX II

Numerical Solution

In order to discretize the equations, some finite difference grids need to be adapted. A cylindrical polar grid did not give a very satisfactory distribution of grid points. Since it is desirable to have a finer mesh near the cylinder surface, the following transformation of the independent variables was made:

$$r = e^{\pi s} \qquad \theta^* = \theta/\pi \ . \tag{II.1}$$

It should be noted that only one-half of the cylinder needs to be considered because of the symmetry and the * notation is dropped for the sake of convenience. In terms of (s, θ) coordinates, the modified vorticity, stream function and the equation of state become:

$$\frac{\partial\omega}{\partial t}+\frac{1}{E^2}[\frac{\partial\Psi}{\partial\theta}\frac{\partial\omega}{\partial s}-\frac{\partial\Psi}{\partial s}\frac{\partial\omega}{\partial\theta}]-\frac{1}{ReE^2}(\frac{\partial^2\omega}{\partial\theta^2}+\frac{\partial^2\omega}{\partial s^2})=\frac{1}{ReE^2}(\frac{\partial^2T_{rr}}{\partial s\partial\theta}+\pi\frac{\partial T_{r\theta}}{\partial\theta}+\frac{\partial^2T_{r\theta}}{\partial\theta^2}-\pi\frac{\partial T_{\theta\theta}}{\partial\theta}-\frac{\partial^2T_{\theta\theta}}{\partial s\partial\theta}-2\pi\frac{\partial T_{r\theta}}{\partial s}-\frac{\partial^2T_{r\theta}}{\partial s^2} \tag{II.2}$$

For the stream function we get:

$$\frac{\partial^2\Psi}{\partial s^2}+\frac{\partial^2\Psi}{\partial\theta^2}=E^2\omega \ , \tag{II.3}$$

where:

$$E = \pi e^{\pi s} \tag{II.4}$$

Similarly, for the constitutive equations we get:

$$[1-\frac{1}{E}\frac{\partial u}{\partial s}(2\lambda_1-\mu_0)]T_{rr}+\lambda_1[\frac{\partial T_{rr}}{\partial t}+\frac{u}{E}\frac{\partial T_{rr}}{\partial s}+\frac{v}{E}\frac{\partial T_{rr}}{\partial\theta}]-\frac{2\lambda_1}{E}\frac{\partial u}{\partial\theta}T_{r\theta}+\frac{\mu_0}{E}\frac{\partial u}{\partial s}T_{\theta\theta}=\frac{2(\lambda_2-\lambda_1)}{E^2}\{E\frac{\partial^2u}{\partial s\partial t}+u\frac{\partial^2u}{\partial s^2}-\pi u\frac{\partial u}{\partial s}+v\frac{\partial^2u}{\partial s\partial\theta}-2(\frac{\partial u}{\partial s})^2-\frac{\partial u}{\partial\theta}\frac{\partial v}{\partial s}+v\pi\frac{\partial u}{\partial\theta}-(\frac{\partial u}{\partial\theta})^2\} \ , \tag{II.5}$$

$$[1+\frac{1}{E}\frac{\partial u}{\partial s}(2\lambda_1-\mu_0)]T_{\theta\theta}+\lambda_1[\frac{\partial T_{\theta\theta}}{\partial t}+\frac{u}{E}\frac{\partial T_{\theta\theta}}{\partial s}+\frac{v}{E}\frac{\partial T_{\theta\theta}}{\partial\theta}]-2\lambda(\frac{\partial v}{\partial s}-\pi v)\frac{T_{r\theta}}{E}-\frac{\mu_0}{E}T_{rr}\frac{\partial u}{\partial s}=\frac{2}{E^2}(\lambda_2-\lambda_1)\{-E\frac{\partial^2u}{\partial s\partial t}-u\frac{\partial^2u}{\partial s^2}+3u\pi\frac{\partial u}{\partial s}-v\frac{\partial^2u}{\partial\theta\partial s}-(\frac{\partial v}{\partial s})^2+2v\pi\frac{\partial v}{\partial s}-\frac{\partial u}{\partial\theta}\frac{\partial v}{\partial s}-v^2\pi^2+v\pi\frac{\partial u}{\partial\theta}+2\frac{\partial v}{\partial\theta}\frac{\partial u}{\partial s}\} \ , \tag{II.6}$$

$$T_{r\theta}+\lambda_1[\frac{\partial T_{r\theta}}{\partial t}+\frac{u}{E}\frac{\partial T_{r\theta}}{\partial s}+\frac{v}{E}\frac{\partial T_{r\theta}}{\partial\theta}]-\frac{\lambda_1}{E}\frac{\partial u}{\partial\theta}T_{\theta\theta}-\frac{\lambda_1}{E}T_{rr}(\frac{\partial v}{\partial s}-\pi v)+\frac{\mu_0}{2E}(T_{rr}+T_{\theta\theta})(\frac{\partial v}{\partial s}-\pi v+\frac{\partial u}{\partial\theta})=\frac{(\lambda_2-\lambda_1)}{E^2}\{E\frac{\partial^2u}{\partial t\partial s}-\pi E\frac{\partial v}{\partial t}+E\frac{\partial^2u}{\partial\theta\partial t}+u(\frac{\partial^2v}{\partial s^2}-3\pi\frac{\partial v}{\partial s}+2v\pi^2+\frac{\partial^2u}{\partial\theta\partial s}-2\pi\frac{\partial u}{\partial\theta})+v(\frac{\partial^2v}{\partial\theta\partial s}+\frac{\partial^2u}{\partial\theta^2}+3\pi\frac{\partial u}{\partial s})-3\frac{\partial u}{\partial s}\frac{\partial v}{\partial s}+\frac{\partial u}{\partial s}\frac{\partial u}{\partial\theta}-\frac{\partial v}{\partial\theta}\frac{\partial v}{\partial s}-\frac{\partial v}{\partial\theta}\frac{\partial u}{\partial\theta}\} \tag{II.7}$$

The modified boundary conditions become:

stream function:

$$\Psi = \partial\Psi/\partial r = 0 \qquad r = a$$
$$\Psi = r\sin\theta \qquad r = R_\infty$$
$$\Psi = 0 \qquad \theta = 0, \pi \ ,$$

vorticity:

$$\omega = 0 \qquad r = R_\infty$$
$$\omega = (8\Psi_{i2} - \Psi_{i3})/2\Delta r^2 \qquad r = a$$
$$\omega = 0 \qquad \theta = 0, \pi \ ,$$

stresses:

$$\begin{aligned} &T_{rr} = T_{\theta\theta} = T_{r\theta} = 0 && r = R_\infty \\ &T_{rr} = 0 && r = a \\ &T_{r\theta} = 0 && \theta = 0, \pi \ . \end{aligned} \quad \text{(II.8)}$$

The vorticity boundary condition on the surface is obtained from the values of stream function near the wall in terms of the Taylor expansion. The "i" in the vorticity equation is the number of nodes in the θ direction.

Making use of the velocity boundary condition, the continuity equation and the definition of vorticity, the boundary conditions for the stress components are given as follows:

$$u = v = \partial v/\partial\theta = \partial u/\partial\theta = \partial u/\partial s = 0$$

$$T_{rr} = 0$$

$$T_{\theta\theta} + \lambda_1 \frac{\partial T_{\theta\theta}}{\partial t} = \frac{2}{E^2}(\lambda_2 - \lambda_1)\{-(\frac{\partial v}{\partial s})^2\} + \frac{2\lambda_1 T_{r\theta}}{E}\frac{\partial v}{\partial s} \ ,$$

$$T_{r\theta} + \lambda_1 \frac{\partial T_{r\theta}}{\partial t} = \frac{\lambda_2 - \lambda_1}{E^2}\{E\frac{\partial^2 v}{\partial s \partial t}\} - \frac{\mu_\circ}{2E}\frac{\partial v}{\partial s} T_{\theta\theta} \ . \quad \text{(II.9)}$$

Boundary conditions on the symmetry line:

$$v = \frac{\partial v}{\partial s} = \frac{\partial u}{\partial \theta} = \frac{\partial}{\partial s}(\frac{\partial u}{\partial \theta}) = 0 \ ,$$

$$[1 - \frac{1}{E}\frac{\partial u}{\partial s}(2\lambda_1 - \mu_\circ)]T_{rr} + \lambda_1(\frac{\partial T_{rr}}{\partial t} + \frac{u}{E}\frac{\partial T_{rr}}{\partial s}) + \frac{\mu_\circ}{E}\frac{\partial u}{\partial s} T_{\theta\theta} = \frac{2(\lambda_2 - \lambda_1)}{E^2}\{E\frac{\partial^2 u}{\partial s \partial t} + u\frac{\partial^2 u}{\partial s^2} - \pi u\frac{\partial u}{\partial s} - 2(\frac{\partial u}{\partial s})^2\} \ ,$$

$$[1 + \frac{1}{E}\frac{\partial u}{\partial s}(2\lambda_1 - \mu_\circ)]T_{\theta\theta} + \lambda_1(\frac{\partial T_{\theta\theta}}{\partial t} + \frac{u}{E}\frac{\partial T_{\theta\theta}}{\partial s}) - \frac{\mu_\circ}{E}\frac{\partial u}{\partial s} T_{rr} = \frac{2}{E^2}(\lambda_2 - \lambda_1)(-E\frac{\partial u}{\partial s \partial t} - u\frac{\partial u}{\partial s^2} + 3u\pi\frac{\partial u}{\partial s} + 2\frac{\partial u}{\partial \theta}\frac{\partial u}{\partial s}) \ . \quad \text{(II.10)}$$